Applied Clay Science 224 (2022) 106515

Contents lists available at ScienceDirect

Applied Clay Science

journal homepage: www.elsevier.com/locate/clay

HRTEM evidences of Tajo Basin mineralogical complexity: Crystal chemistry and genetic relationship

Emilia García-Romero [a,b,*], Mercedes Suárez [c]

[a] Department of Mineralogy and Petrology, Complutense University of Madrid, 28040 Madrid, Spain
[b] Geosciences Institute (IGEO), Spanish Research Council and Complutense University (CSIC-UCM), 28040 Madrid, Spain
[c] Department of Geology, University of Salamanca, 37008 Salamanca, Spain

ARTICLE INFO

Keywords:
Tajo Basin
HRTEM
Bentonite
Saponite
Mixed-layer
Hydroxy-interlayered mineral

ABSTRACT

In this study, a new genetic interpretation of the Mg-bentonite deposits from the Tajo Basin is given through a high-resolution transmission electron microscopy study. These bentonites, belonging to the Green Clays and Pink Clays lithostratigraphic units, are afforded by the sum of processes occurring during the weathering of parent rocks and the evolution of the materials by the transformation of phyllosilicates in the sedimentary environment. The primary phyllosilicates progressively change their microstructure and crystal chemistry, resulting in very complex clay minerals assemblages. The Green Clays are relatively enriched in Al, Fe, and K, whereas Pink Clays are enriched in Mg and Si, corresponding to almost pure trioctahedral smectites. Although the point analysis of the particles showed a continuous compositional variation that evidences their genetical relationship, they were statistically classified in groups that represented the evolution from the primary phyllosilicates (dioctahedral and trioctahedral micas and chlorites) to the final products comprise very low-charge saponite and scarce sepiolite. The intermediate steps in this transformation included the following: 1) particles of structural formulas with an excess of octahedral cations that were interpreted as hydroxy-interlayer minerals and 2) random mixed-layers of illite/smectite progressively poorer in illitic component as the more evolved particles. Green Clays correspond to the state of transformation to smectites where partially transformed detrital components were still predominant, corresponding to more proximal facies, whereas Pink Clays represented most evolved stages in the mineral transformation. The alternation of Green and Pink Clay levels was related to climatic changes with alternation of wetter and drier periods.

1. Introduction

Weathering reactions of rocks on the Earth's surface are responsible for producing abundant clay minerals—mainly kaolinite and smectites. During weathering, a remarkable suite of transitional phases such as vermiculite and several interstratifications with vermiculitic, smectitic, chloritic and micaceous layers develop. Smectites in surface environments mainly form by the weathering of pre-existing minerals and grow under very different conditions. The mechanisms of smectite formation include neoformation and transformation, which have been widely studied in the literature (Wilson, 2004; Meunier, 2005; Velde and Meunier, 2008; Pozo and Galán, 2015; García-Romero and Suárez, 2021; and references therein). Mica and chlorite in sedimentary environments can alter, leading the formation of Fe-oxides, vermiculite, and/or smectite. Several researchers have studied the process and products of the alteration of both mica, particularly biotite, and chlorite by observing naturally altered materials (Romero et al., 1992; Aspandiar and Eggleton, 2002) and those weathered artificially in the laboratory (Correns, 1963; Robert, 1973; Robert and Barshad, 1973; Malström and Banwart, 1997, among others).

There is a general agreement that smectite formation via mica weathering starts with the release of interlayer K^+, which implies a gradual opening of illite interlayers to vermiculite or smectite interlayers as well as an increase in Si. The charge of the layer decreases, causing the opening of the interlayer space and the entering of polar molecules (water or organic molecules). Biotite is less resistant to weathering than muscovite, and their natural weathering involves other structural changes as well, such as the oxidation of Fe^{2+} and its ejection from octahedral sheets of ferric ions leading to a more dioctahedral structure (Robert, 1973; Banfield and Eggleton, 1988; Kogure and

* Corresponding author at: Department of Mineralogy and Petrology, Complutense University of Madrid, 28040 Madrid, Spain.
E-mail address: mromero@ucm.es (E. García-Romero).

https://doi.org/10.1016/j.clay.2022.106515
Received 9 February 2022; Received in revised form 30 March 2022; Accepted 4 April 2022
Available online 22 April 2022

Murakami, 1996; Malström and Banwart, 1997, and Wilson, 2004). Most researchers of natural mica-to-smectite alteration argued that transformation reactions occur through mixed-layers of illite/smectite (Güven and Kerr, 1966; Rimmer and Eberl, 1982; Ross et al., 1982; Srodón and Eberl, 1984; Banfield and Eggleton, 1990; Suarez et al., 1994, Elsass et al., 1997; Klimentidis, 1986; Veblen et al., 1990; Wilson, 2004, among others).

Smectite can be formed also by chlorite alteration (Hervillon and Makumbi, 1975; Ross et al., 1982; Proust et al., 1987; Buurman et al., 1988). The transformation of chlorite to smectite is chemically characterized by Fe and Mg losses with a slight decrease in the Al/Si ratio as well as the formation of Fe minerals (Ross et al., 1982; Mukarami et al., 1996). The oxidation of ferrous iron causes the partial loss of octahedral cations and the preferential dissolution of brucite sheets. This transformation occurs through mixed-layers, and the most noteworthy step of this alteration is the formation of regular chlorite/vermiculite mixed-layers, with a corrensite-type structure (Meunier, 2005), followed by irregularly mixed-layer chlorite/vermiculite (Proust et al., 1987; Proust, 1982; Hervillon and Makumbi, 1975) or vermiculite/smectite (Craw, 1984).

According to Barnhisel (1977), common secondary products of the chemical weathering of phyllosilicates include metal oxides and hydroxy-interlayered minerals (HIMs). Predominantly, HIMs comprise at least partially expansible 2:1 phyllosilicates such as mica, smectite, and vermiculite with mostly Al oligomers in the interlayer. HIMs, such as hydroxyl-interlayered smectite (HIS) or hydroxy-interlayered vermiculite (HIV), are typical weathering products in acidic soils, containing varying amounts of $Al[(OH)_x,(H_2O)_y]^{3-x}$ polymers in the interlayer space (Barnhisel and Bertsch, 1989). Apart from Al^{3+}, other metal cations such as Mg^{2+} and $Fe^{2+/3+}$ may similarly produce intercalated oligomers (Dixon and Jackson, 1962; Gupta and Malik, 1969).

The Tajo Basin has considerable deposits of sedimentary bentonites. Thus, the aim of this work is to perform an in-depth study of the crystal chemistry of the smectites and characterize their genetic relationship with other phyllosilicates through high-resolution transmission electron microscopy (HRTEM).

2. Geological background

Significant bentonite deposits of the Miocene age (Aragonian-Vallesian) occur in the Tajo Basin, which is a complex intracratonic basin located in the center of the Iberian Peninsula. It formed through intense Cenozoic Alpine deformation within the Iberian microplate driven by the Africa–Eurasia collision. The basin has a triangular shape and is limited by mountain ranges (Fig. 1a supplementary material), which were the source areas of the sediments that filled the basin: 1) the Central System to the northwest, formed by igneous (mainly leucogranites, monzoleucogranites, and granodiorites and others as granites, quartzdiorites, and syenites) and metamorphic (slates, schists, and gneisses) rocks of Paleozoic age; 2) the Iberian Range to the northeast, which is mainly composed of carbonate and evaporitic Mesozoic rocks; and 3) the Toledo Mountains, also formed by granitic and high-grade metamorphic rocks, to the south. The mineralogy of the basin reflects that of their source area, which was rich in chlorite, biotite, and muscovite (principally from the metamorphic rocks) in addition to quartz and feldspars.

There are three Miocene units separated by unconformities from the underlying Units in the Tajo Basin: the Lower, Intermediate, and Upper Units (Junco and Calvo, 1983; Calvo et al., 1989a; Calvo et al., 1993; Alonso-Zarza et al., 2004), and they comprise various alluvial and lacustrine deposits, which are arranged in a complex concentric pattern characteristic of a lake basin that is both hydrologically and topographically closed (Ordoñez et al., 1991). Deposits of bentonites are located within the Intermediate Unit, in the so-called Green Clays

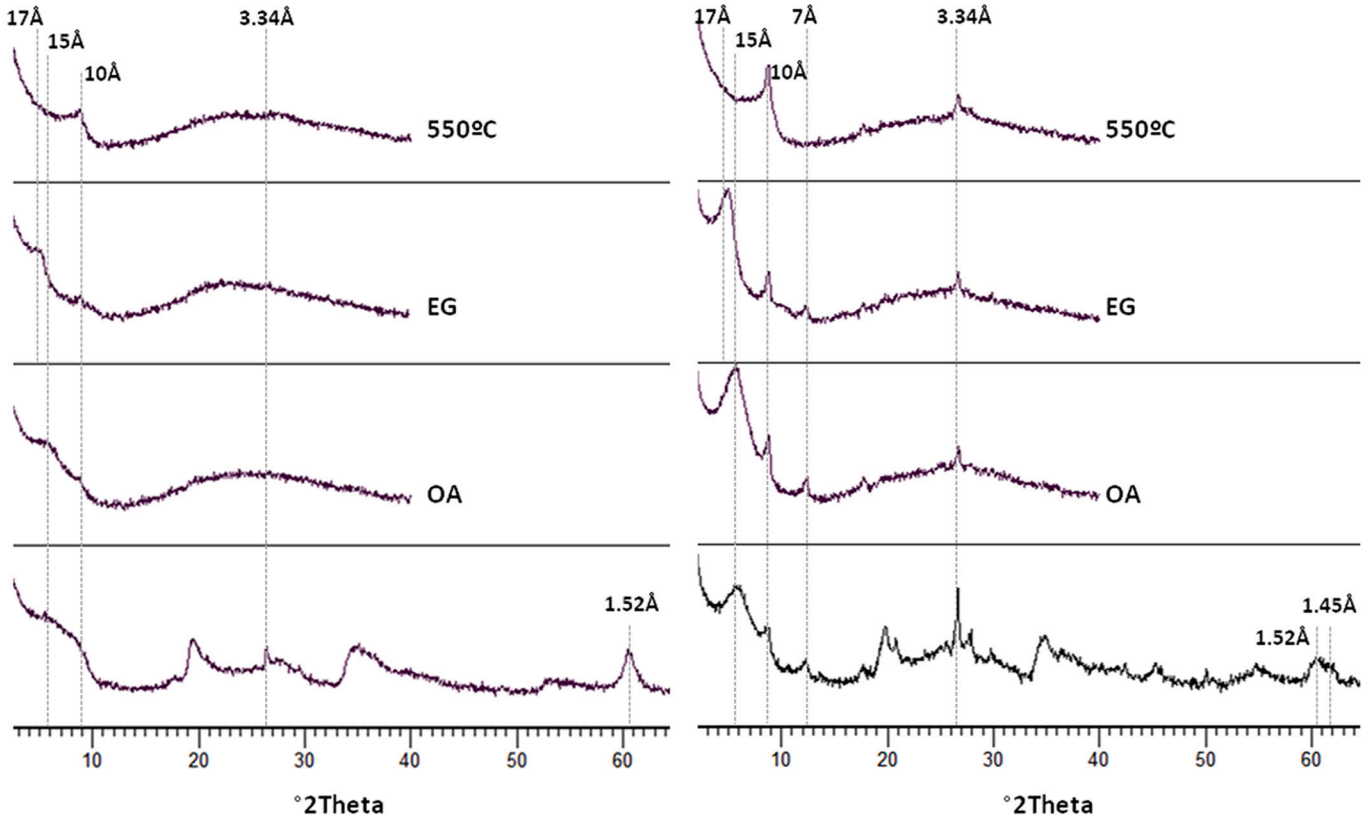

Fig. 1. Representative X-Ray diffractograms of Pink Clays (left, ROS sample) and Green Clays (right, ESB 11 sample). OA: oriented aggregate. EG: ethylene glycol. 550 °C: heated at 550 °C. (For interpretation of the references to colour in this figure legend, the reader is referred to the web version of this article.)

lithostratigraphic unit, which contains alternating Green and Pink Clays. These were deposited along the margins of the evaporitic core of the basin in a low-energy sedimentary environment, occurring as mudflat facies (Brell et al., 1985; Doval et al., 1985; Calvo et al., 1989b; García-Romero et al., 2019).

In general, the Green Clay Unit comprises bentonites that consist alternating greenish massive clays. At the top of this unit appear dolomitic marls or dolostones that are locally silicified. Toward the lower–middle part, the bentonitic clays contain some beds of micaceous sands showing crossed- or parallel-lamination whit biotite and chlorite as the only phyllosilicates in these sands; several interbedded pinkish clay levels (Pink Clays bentonites), sometimes containing sepiolite and isolated carbonatic nodules (Brell et al., 1985; García-Romero et al., 1990; Bellanca et al., 1992; Cuevas et al., 1993; Pozo and Casas, 1999; García-Romero et al., 2019). Presently, these bentonites are mined, with the most important exploitations located south of Madrid Province (Fig. 1a supplementary material), taking advantage of both the Green and the Pink Clays levels.

The Green Clays levels mainly comprise trioctahedral smectites, containing minor amounts of quartz and illite together with scarce feldspar as well as other phyllosilicates such as smectite/chlorite or illite/smectite random mixed-layers, sepiolite, and/or kaolinite (Brell et al., 1985; Domínguez Díaz et al., 1997) However, the Pink Clays are almost pure smectites, and rarely have relicts of detrital minerals such as quartz. Pink Clays have been largely studied, yet there is a lack of agreement on their mineralogical classification. Several authors described these clays as mixed-layer kerolite–stevensite (Martín de Vidales et al., 1991; Pozo and Casas, 1992, 1995; Pozo et al., 1999; Pozo and Casas, 1999; Clauer et al., 2012), kerolite (Pozo and Casas, 1999), stevensite (De Santiago et al., 2000; Cuevas et al., 1993, 2003; García-Rivas et al., 2018), interstratified of turbostratic talc and saponite (Steudel et al., 2017), and finally as low-charge saponite–stevensite following the homoionization of samples with Ca (García-Romero et al., 2021). However, there is agreement on the low crystallinity and structural disorder of these low-charge phyllosilicates.

The Green Clays mineralogical assemblage is explained by the reaction between detrital clay particles coming from weathering of the source area and their alteration products in the sedimentary basin, where they suffered transformation and neoformation processes, whereas the Pink Clays would exhibit authigenic characteristics (Cuevas et al., 1993; Domínguez Díaz et al., 1997; De Santiago et al., 1998; Pozo and Calvo, 2015; García-Rivas et al., 2018; Herranz and Pozo, 2018). The main source areas of the bentonitic materials are the igneous and metamorphic rocks of the Central System, as already stated, but magnesium and silica enrichment occurred during the process of transformation of the detrital minerals that reach the sedimentary basin. The Mg content in the Tajo Basin is remarkable, which appears in saponitic deposits and in very important sepiolite exploitations (Cuevas et al., 2010; García-Romero et al., 2019 and references therein), forming one of the richest basins in Mg in the world.

3. Materials and methods

3.1. Materials

The studied samples corresponded to Green or Grey-Greenish and to Pink Clays, that were massive or of fine parallel lamination and frequent bioturbations. They were collected by taking advantage of the quarry fronts of most economically important exploitations of bentonites in the Tajo Basin, located to the south of Madrid in two areas (Fig. 1b supplementary material): 1) seven samples came from quarries at the bottom of the inselbergs of Cerro del Águila and Cerro de Magán (MCM, ROS, TAJ, VER, VER3, VER19–1, and VER19–2), next to the villages of Magán and Villaluenga, respectively. 2) The other fiveteen samples (ESB2, ESB3, ESB4, ESB5, ESB6, ESB11, ESB21, PB10, PB11, PB12, RESB3, RESB6, RESB11, RESQ, and SES2) were collected from quarries located among the localities of Esquivias, Seseña, and Borox. Both the Green and Pink Clays appeared closely interbedded with each other in the two studied areas. Samples ESB2, ESB3, ESB6, ESB11, EBS21, PB12, SES2, VER, VER3, VER19–1, and VER19–2 corresponded to Green Clays and samples ESB4, ESB5, MCM, PB10, PB11, RESB3, RESB6, RESB11, RESQ, ROS, and TAJ corresponded to Pink Clays.

3.2. Methods

Mineralogical characterization was performed via powder X-Ray diffraction (XRD) of the whole-rock samples powdered using an agate manual mortar as well as <2 μm fractions obtained via decantation and studied as oriented aggregates under ambient conditions after solvation with ethylene glycol and heating at 550 °C. A Bruker D-8 advance XRD diffractometer using CuKα radiation and a graphite monochromator was employed, with a step size of 0.05° 2 theta and a counting time of 1 s per step.

Textural features were established by using scanning electron microscopy (SEM) and high resolution transmission electron microscopy (HRTEM) at the Centro Nacional de Microscopía Electrónica (CNME, Spain). The SEM observations were conducted with a JEOL JSM-6330F (field emission scanning electron microscope) operated at 10 and 20 kV, wd 15 mm, and SEI, equipped with an Oxford Instruments: X-Max 80 mm^2 qualitative elemental analysis by energy dispersion spectroscopy (EDS) at 127 eV and 5.9 keV. Prior to the SEM examination, freshly fractured surfaces of representative samples were air-dried and coated with Au under a vacuum. The HRTEM observations were performed using a JEOL 3000 FX field-emission microscope with a LaB_6 filament at an acceleration voltage of 300 kV with a point-to-point resolution of 0.17 nm. The microscope was equipped with a double-tilt sample holder (with a maximum angle of ±23°) and a CCD camera for digitally recording images. Clay minerals are extremely beam-sensitive compared to other non-hydrated minerals, posing a higher level of difficulty for HRTEM imaging. Therefore, the samples were prepared under special conditions to prevent beam damage. The experimental conditions were optimized to avoid structural modifications using a low beam intensity (<500 counts on the CCD camera) and an exposure time of 0.8 s to acquire the image. In addition, some of the samples were prepared through treatments to preserve the microstructure and avoid the collapse of the smectite interlayer space. These treatments were conducted in a series of successive steps, where a small portion of the sample was placed in agar-agar to protect it from future stains. The sample must be hydrated and the water progressively replaced by methanol; afterward the alcohol was replaced by Spurr resin, according to the methodology proposed by Tessier (1984) and Tessier and Pedro (1987). After polymerization of the resin, thin sections (50 nm) were cut by ultramicrotomy. This procedure minimizes dehydration during HRTEM and thus helped preserve the natural texture of the samples.

The chemical composition of the samples was obtained using analytical electron microscopy (AEM) with HRTEM, both in natural samples and those homoionized with Ca^{2+}. For AEM study, samples were prepared by depositing a drop of diluted clay suspension onto copper grids with a holey carbon film. Thin individual grains of minerals were scattered onto the grid with the (001) planes parallel to the grid holder. The analyses were conducted at two different laboratories: the CNME and the Centro de Instrumentación Científica, University of Granada, Spain (CIC). At the CNME were used two microscopes: a JEOL JEM 1400 microscope, with an acceleration voltage of 100 kV and 0.38 nm point-to-point resolution, and a JEOL 3000-F field-emission microscope with a LaB_6 filament, an acceleration voltage of 300 kV, a point-to-point resolution of 0.17 nm. Both microscopes incorporated an OXFORD ISIS EDX spectrometer (136 eV resolution at 5.39 keV) and an INCA microanalysis suite (Oxford Instruments) equipped with its own software for quantitative analysis. Structural formulas were calculated on the basis of O_{20} $(OH)_4$. All Fe present in the samples was considered Fe^{3+} (owing to the limitation of the technique), but the possible existence of

scarce Fe^{2+} cannot be excluded.

To determine the correct distribution and structural positions of the cations, some samples were homoionized with Ca (ESB2, ESB3, ESB5, ESB6, ESB11, ESB21, RESQ, ROS, SES2, and VER). For this cationic exchange, powdered samples were immersed in a 1 M $CaCl_2$ solution at room temperature for three successive 24-h baths. Afterwards, the chloride solutions were removed, and the samples were washed with successive distilled water and centrifugation baths until the chloride was completely removed. The absence of chloride was confirmed with dilute $AgNO_3$. Thus, the exchangeable cations that the smectites originally contained were replaced by Ca^{2+}.

4. Results

4.1. Mineralogy and chemical composition

In agreement with the aforementioned previous studies of the Tajo Basin, the XRD patterns showed than the Green Clays mainly comprise smectites which have wide reflections (Fig. 1). The samples sometimes contain minor amounts of illite, kaolinite, quartz, feldspars, and occasionally calcite. At times, they showed scarce chlorite and low-intensity diffraction effects between d-spacings of 10 and 15 Å, or minor broad peaks in the long-angle region of the powder patterns (more than 15 Å) with no defined maxima, which indicated the presence of either a wide range of random mixed-layers or 2:1 intermediate phases in which smectite and illite were dominant. The presence of minor mixed-layer phases was also supported by the asymmetry of the reflections, principally those of illite, which showed its 10 Å reflection open to a higher d-spacing. The d-spacing of the 060 reflection showed a band with two maxima at 1.49 and 1.52 Å, thus indicating the coexistence of dioctahedral and trioctahedral phases or domains in the same sample. The XRD patterns of the Pink Clays showed significant differences (Fig. 1). They were trioctahedral, as the 060 reflection at 1.52 Å indicated. Although they were very pure smectites, there was not a clear 001 reflection; only hk0 reflections appeared in the powder XRD patterns, together with a very broad diffraction effect at low angles between 3° 2Θ and 9° 2Θ. This wide effect implies the existence of crystalline plains with variable d-spacing diffraction, between 10 Å and more than 20 Å, without ordering in the [001] direction. The XRD patterns of the oriented aggregates showed this wide effect, which changed slightly, moving to lower angles, when the samples were solvated with ethylene glycol, indicating a certain swelling ability. Further, when the oriented aggregates were heated at 550 °C, the higher d-spacings collapsed, and a very broad peak at ~10 Å appeared, although in some samples, small peaks between 10 Å and 14 Å appeared, which were related to the presence of some chlorite layers.

The point chemical data obtained by AEM analyses of isolated particles of the natural and Ca-homoionized samples (both Green and Pink Clays,) displayed a broad compositional variability (Tables 1 and 2 supplementary material), despite all analyses being performed on representative particles of characteristic smectitic morphology, as shown in the next section. The oxide percentages of the samples showed a remarkably high standard deviation, mainly in the Green Clays (Table 1), which was related to the continuous compositional variations in the particles in all studied samples. The chemical composition of Green Clay and Pink Clay particles showed noteworthy differences. The maximum and minimum of oxide percentages varied among the samples (Table 1), but even more significant were the mean values. The Pink Clay samples were richer in MgO (mean = 30.54%) than the Green Clays (mean = 18.40%) and poorer in Al_2O_3 (2.42% and 13.66%, respectively). In the same way, the mean values of K_2O and Fe_2O_3 were higher in the Green Clays (1.66% and 5.32%, respectively) than those in Pink Clays (0.18% and 0.81%, respectively). Although there was a difference in the composition of Pink and Green Clays, particles with similar composition were found in both types of rocks, but they appeared in different proportions. Particles richer in Si and Mg were more abundant in Pink Clays, while those richer in Al, Fe, and K were much more frequent in Green Clays. In addition, the variability of the composition of the laminar particles in these bentonites, both in Green and Pink Clays was an intrinsic characteristic of all samples, and it was not because of

Table 1
Maximum (Max), Minimum (Min), Mean and Standard Deviation (St. Dv.) values of the main oxides percentage (%), of natural and homoionized with Ca both Green and Pink samples. N: number of samples analyzed.

		SiO_2	Al_2O_3	Fe_2O_3	MgO	CaO	K_2O
Green Clays	Max	69.65	36.82	21.88	32.73	4.39	6.93
$N = 247$	Min	39.80	2.51	0.00	2.72	0.00	0.00
	Mean	**60.20**	**13.66**	**5.32**	**18.40**	**0.54**	**1.66**
	St. Dv.	4.71	7.54	4.18	8.85	0.61	1.56
Ca Green	Max	72.96	37.43	29.57	32.94	9.88	10.51
Clays	Min	40.55	2.74	0.00	1.24	0.00	0.00
$N = 193$	**Mean**	**58.33**	**18.24**	**6.51**	**13.11**	**1.59**	**2.05**
	St. Dv.	6.02	7.47	4.96	7.88	0.96	1.89
Pink Clays	Max	75.75	17.34	9.10	35.82	2.26	2.80
$N = 189$	Min	54.86	0.00	0.00	17.41	0.00	0.00
	Mean	**65.70**	**2.42**	**0.81**	**30.54**	**0.34**	**0.18**
	St. Dv.	2.99	3.11	1.30	3.83	0.37	0.40
Ca Pink Clays	Max	77.08	9.25	5.64	35.38	7.97	2.02
$N = 140$	Min	59.16	0.00	0.00	14.69	0.21	0.00
	Mean	**64.86**	**1.74**	**0.70**	**31.18**	**1.44**	**0.07**
	St. Dv.	2.70	1.66	0.93	3.41	0.94	0.28

Table 2
Chemical composition (mean values, wt% major oxides) and structural formulae of the groups obtained after the cluster analysis by the Ward Method. Numbers of cations on the basis $O_{20}(OH)_4$.

Mean analyses (% major oxides)						
	A1 MEAN	A2 MEAN	B1 MEAN	B211 MEAN	B212 MEAN	B22 MEAN
MgO	9.68	6.4	23.93	33.37	30.89	26.76
St. Dv.	3.24	2.86	3.84	1.02	0.98	4.2
Al_2O_3	22.15	22.2	8.58	1.01	2.58	1.1
Al St. Dv.	3.79	6.11	2.81	0.44	1,00	0.97
SiO_2	53.84	63.5	62.06	63.88	64.35	69.38
Si St. Dv.	4.36	5.11	2.13	0.8	1.22	3.15
K_2O	2.88	2.04	0.68	0.01	0.09	0.02
K St. Dv.	1.71	2.26	0.55	0.04	0.21	0.06
CaO	1.61	1.13	1.95	1.19	1.38	2.05
Ca St. Dv.	0.77	0.55	1.45	0.29	0.4	1.55
Fe_2O_3	9.56	4.58	2.8	0.53	0.71	0.67
Fe St. Dv.	5.15	2.47	1.53	0.52	0.92	1.17
TiO_2	0.27	0.16	0,00	0.00	0.00	0.00
Ti St. Dv.	0.5	0.67	0.00	0.00	0.00	0.00
Structural formulas. Numbers of cations on the basis $O_{20}(OH)_4$						
Si	6.73	7.60	7.56	7.76	7.79	8.32
Al	1.27	0.40	0.44	0.14	0.21	
Fe^{3+}				0.05		
Σ tet.	8.00	8.00	8.00	8.00	8.00	8.32
Al	1.99	2.73	0.79		0.16	0.16
Fe^{3+}	0.90	0.41	0.26		0.06	0.06
Mg	1.80	1.14	4.34	6.04	5.58	4.78
Ti	0.03	0.01				
Σ oct.	4.72	4.29	5.39	6.04	5.80	5.00
Ca	0.22	0.14	0.25	0.15	0.18	0.26
K	0.46	0.31	0.11		0.06	
Tet. Ch.	−1.27	−0.40	−0.44	−0.39	−0.21	0.32
Oct. Ch.	0.39	−0.26	−0.17	0.08	−0.18	−1.78
L. Ch.	−0.88	−0.66	−0.61	−0.31	−0.39	−1.46

St. Dv.: Standard deviation. Σ tet.: number of tetrahedral cations. Σ oct.: number of octahedral cations. Tet. Ch.: Tetrahedral charge. Oct. Ch.: Octahedral charge. L. Ch.: Layer charge.

the sum of the analyses of different samples because the same, very wide variations existed in each sample. Moreover, the assemblages of the values for all oxides of the main major elements (Si, Al, Fe, and Mg) showed a continuous variation from highest to lowest values (Fig. 2).

To properly fit the smectite structural formulas, the samples were homoionized with Ca^{2+} (García-Romero et al., 2021) to unequivocally determine the Mg allocation. When the point analyses of natural and homoionic samples were compared, the general trends obtained were the same, with the continuous compositional variation that was discussed previously (Table 1, Fig. 2). Although the mean content of MgO% decreased in the homoionic Green Clays, because the interlayer Mg was changed by Ca, however, this did not happen in Pink Clays because they were very Mg-rich clays with a low layer charge and interlayer cations. Nevertheless, while K_2O% almost reached zero in the homoionic Pink Clays, the mean K_2O% content did not decrease in the homoionic Green Clays, indicating the presence of interstratified mica layers (Hoang-Minh et al., 2019; García-Romero et al., 2021).

4.2. Statistical analysis

Significant correlations existed among the percentages of different oxides of major elements (Table 3 supplementary material). Al_2O_3 and Fe_2O_3 percentages were positively correlated with each other, and both were negatively correlated with MgO and positively correlated with K_2O, while SiO_2 correlated positively with MgO. Furthermore, there was a continuous compositional variation, as shown in Fig. 2, where the percentages of elements are plotted. The high standard deviation (Table 1) reflects the high compositional variability of both Green and Pink Clays, which is a consequence of the mixture of particles with different crystal-chemistry. This compositional variation made it

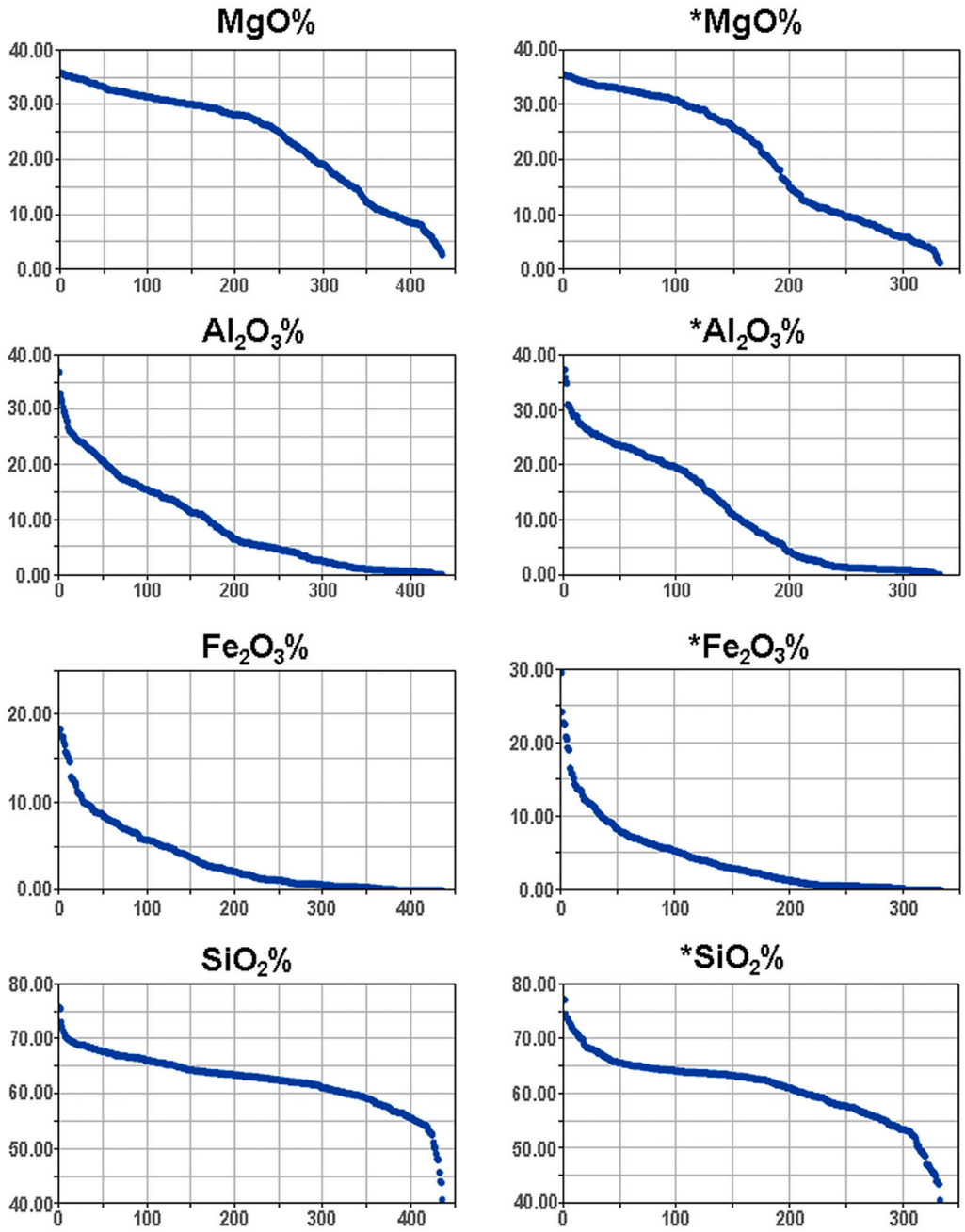

Fig. 2. Oxide content of the major elements ordered from the highest to lowest values. The left column corresponds to natural samples, while the right column (indicates with *) correspond to homoionic samples. The same tendencies and the continuous variations in all oxides are observed in the two groups of plots.

difficult to determine representative structural formulas for groups of minerals because the individual point analyses corresponded to very different chemical compositions with high standard deviations. A very high proportion of point analyses did not fit properly for 2:1 minerals: 10.1% with more than eight Si atoms per unit cell (p.u.c.), 12.8% with more than six atoms p.u.c. in octahedral positions, and 47.4% with excess octahedral charge (Oct. Ch.). However, several compositional groups could be distinguished from the statistical analysis of the chemical data.

A classification of the analyzed particles in the homoionic samples was performed using cluster analysis by the Ward Method, and the obtained groups are identifiable when SiO_2 and MgO are plotted (Fig. 3 and Fig. 2 supplementary material). Firstly, the points were grouped into A and B groups. Subgroups were obtained and named A1, A2, B1, and B2, and this last group was formed by B21 (B211 and B212) and B22 (Fig. 2 supplementary material). As is logical, these groups and subgroups had common characteristics that were more easily deduced from their mean chemical compositions (Table 2). The group A particles had a high content of Al_2O_3, Fe_2O_3, and K_2O, with the A1 group being richer in MgO and Fe_2O_3 than A2. The B group was characterized by the highest MgO content, and differences among the subgroups in B were related to an intermediate content of in Al_2O_3, Fe_2O_3, and K_2O, a maximal content of SiO_2 in B22, and a maximal content of MgO in B211 and B212. K_2O was related to the A1, A2, and B1 groups.

From these mean compositions, the structural formula of each subgroup can be fitted as 2:1 phyllosilicate (Table 2). The interlayer of the A1, A2, and B1 groups contain K^+, indicating the presence of illite layers, as previously said. However, they have different tetrahedral Al substitution and very different octahedral content. The analyzed particles of group A are mainly dioctahedral, since the number of octahedral cations (Σ oct.) is 4.72 and 4.29 for A1 and A2, respectively. A1 has a layer charge (L. Ch.) of −0.88 and its mean structural formula allows us to classify it as illite with excess octahedral charge. The mean structural formula of group A2 corresponds to a dioctahedral structure, and it has −0.66 L. Ch., mainly located at the tetrahedral sheet; therefore, it should be classified as beidellite. B1 fits as an intermediate between di- and trioctrahedral smectite (0.61 L. Ch. and 5.39 Σ oct.). However, groups B211 and B212 correspond to trioctahedral smectites (saponite), while B22 does not fit any 2:1 phyllosilicate (Table 2). Although no particle with fibrous morphology was analyzed, considering its high content of Si and Mg, the structural formula of the mean chemical composition of B22 fited as sepiolite, that is to say, $O_{30}(OH)_4$. In this case, the formula fits better, but it is not a perfect fit (Si_{12} $Mg_{4.78}$ $Al_{0.16}$ $Fe^{3+}_{0.06}$ O_{30} $Ca_{0.26}$ $(OH)_4$).

4.3. Micromorphological features

Overall, the SEM images of the Green Clays were consistent with a detrital origin. The samples had an isotropic fabric, formed by a random (no oriented) array of particles deposited in a massive flocculated fabric, which hardly ever reached more than a few micrometers. They had a flaky morphology and undulating edges in a mess arrangement in edge-to-face and edge-to-edge contacts, resulting in a disordered "cornflake" microstructure. Scarce detrital grains remain included in the smectite mass, mainly of quartz and sometimes larger altered platelets of micas and/or chlorites (Fig. 4a, b). These large platelets were undulated with open edges owing to growth of smectite, and they were covered by smaller particles that grew on their surfaces (Fig. 4c). The Pink Clays samples showed some different textural features. They had a remarkably open microstructure, where very small smectite particles were arranged, resulting in a very open and homogeneous distribution of particles that showed a tendency to be connected, forming flocs or aggregate structures with pseudospherical morphologies (Fig. 4d, e) separated by pseudopolygonal voids of varying sizes and shapes (Fig. 4f) resulting in a "cornflake" and "honeycomb" microstructure. Occasionally, the smectite particles of both Green and Pink Clays samples exhibited fibrous ends that corresponded to the growth of sepiolite fibers (Fig. 4g, h); these laminar particles have a composition closer to sepiolite than that to smectite (group B22), as discussed in the previous section.

Under HRTEM inspection, particles from both the Pink and Green Clays appeared as a mixture of aggregates of small nanoparticles with variable morphology as much up to a few hundred nanometers in lateral length, which, at the same time were made up of smaller lenticular nanoparticles. Individual nanoparticles were continuously curved with a general wavy and pointy appearance and sometimes twister ends with no clear grain boundary between separate crystals, which appeared as rolled-up edges (Fig. 5 a-d) of extremely thin films formed as the result of edge-to-edge aggregation of particles, as described by García-Romero

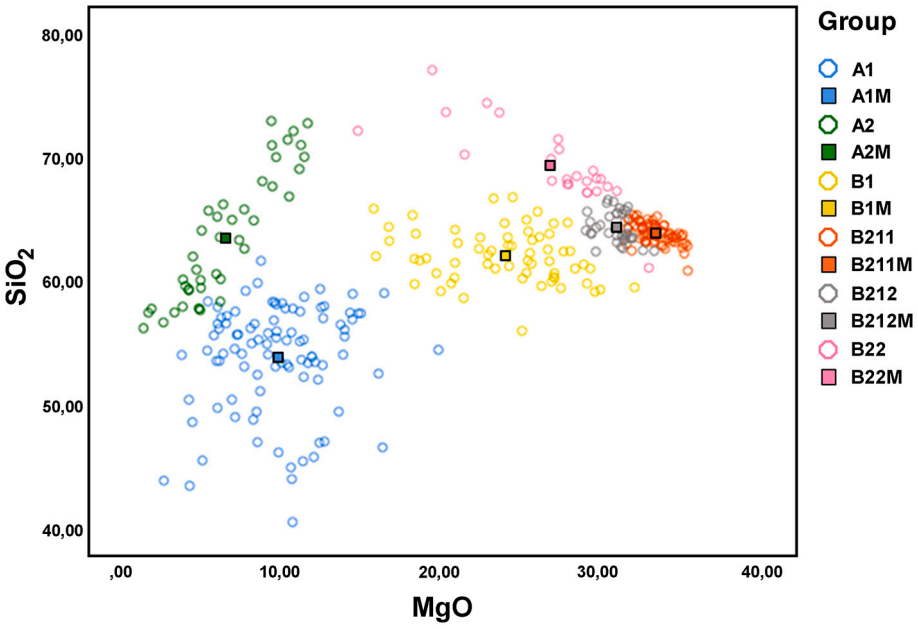

Fig. 3. Binary plot of SiO_2 versus MgO of all analyzed points for Ca-homoionized samples. Colour corresponds to the groups defined from the cluster analysis according to the legend. Square points correspond to the mean value for each group.

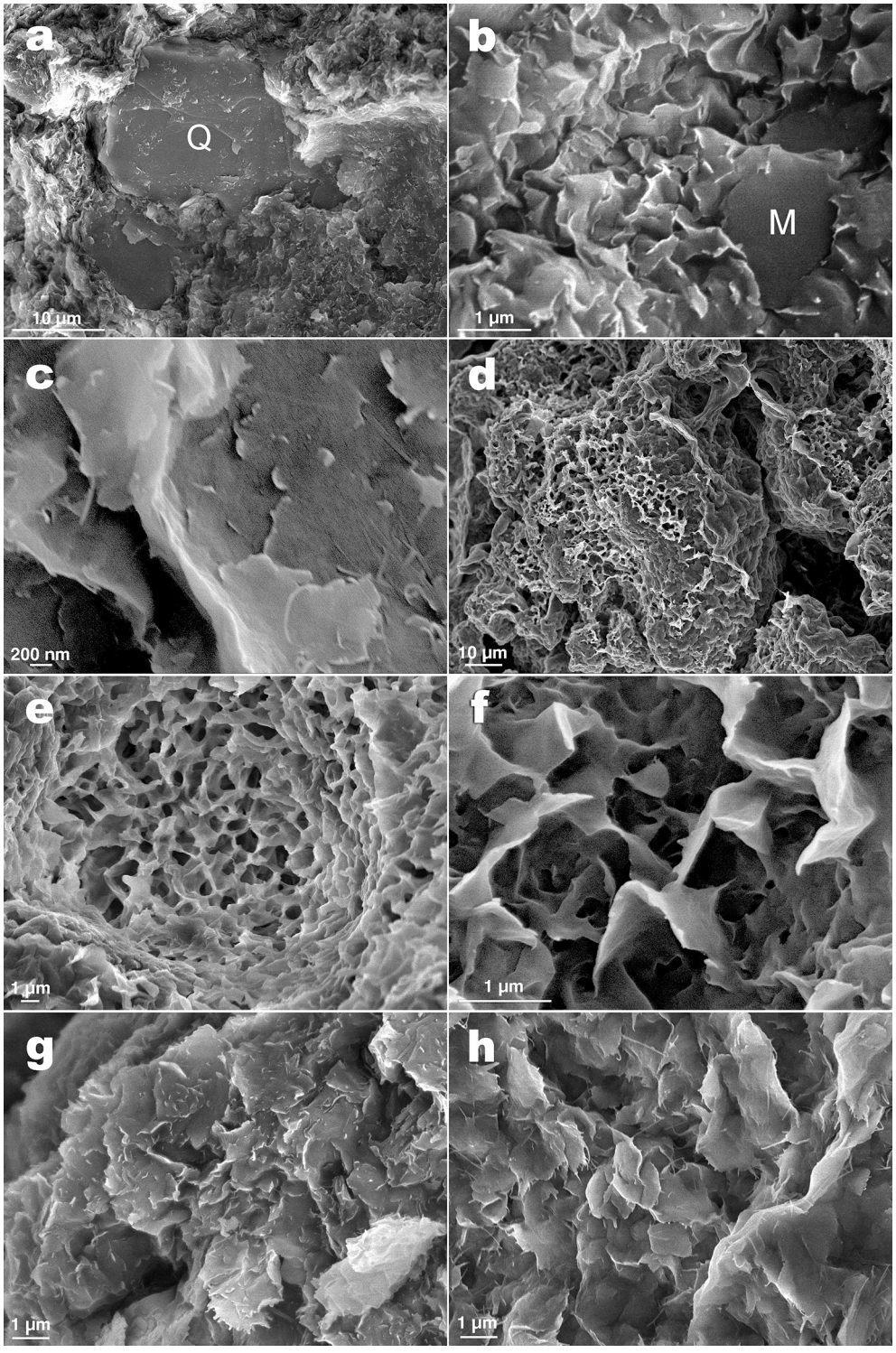

Fig. 4. Representative SEM images of isotropic fabric, formed by a random array of particles disposed in a massive flocculated fabric from Green Clays (a, b, c, g) and Pink Clays (d, e, f, h). a, b) detrital grains included in the smectite mass. c) large platelet with undulated edges covered by smaller particles growing on their surface. d, e) smectite particles arranged in a very open microstructure with pseudopolygonal voids, forming flocs or aggregate structures with pseudospherical morphologies f) detail of pseudopolygonal voids. g, h) mass of smectite particles with undulated and fibrous ends. Q: Quartz, M: Mica. (For interpretation of the references to colour in this figure legend, the reader is referred to the web version of this article.)

and Suárez (2018). The particles of the Pink Clays samples were remarkably smaller than those Green Clay samples (Fig. 5c, d). They comprised only a few layers, which agrees with the extreme poor crystallinity and the lack of stacking found in the XRD patterns (Fig. 1). Steudel et al. (2017) also reported very small particle sizes as one characteristic of this bentonite.

The lattice-fringe images showed the dominant clay mass as being a disorganized, imperfect, wavy, anastomosing, and discontinuous lattice fringe. The lack of staking in the [001] direction and the edge dislocations were characteristic of these samples. The d-spacing varied from 10 to more than 20 Å in disordered domains of only a few layers, with scarce lateral continuity and local variation in layer width, as clearly shown in Fig. 6a, c. The anastomosing lattice-fringe images of smectite-like nanoparticles typically exhibited changes in image contrast along layers owing to small orientation changes in the crystal. The samples occasionally contained small packets of only a few relatively defect-free 10 Å layers (Fig. 5e) and scarce chlorite (14 Å) layers (Fig. 6b) within the disordered smectitic mass. The residual illitic crystals were scarce, but they appeared in all the Green Clay samples, as well as the Pink Clays, although less prominently. The restitic chlorite of only was found in the

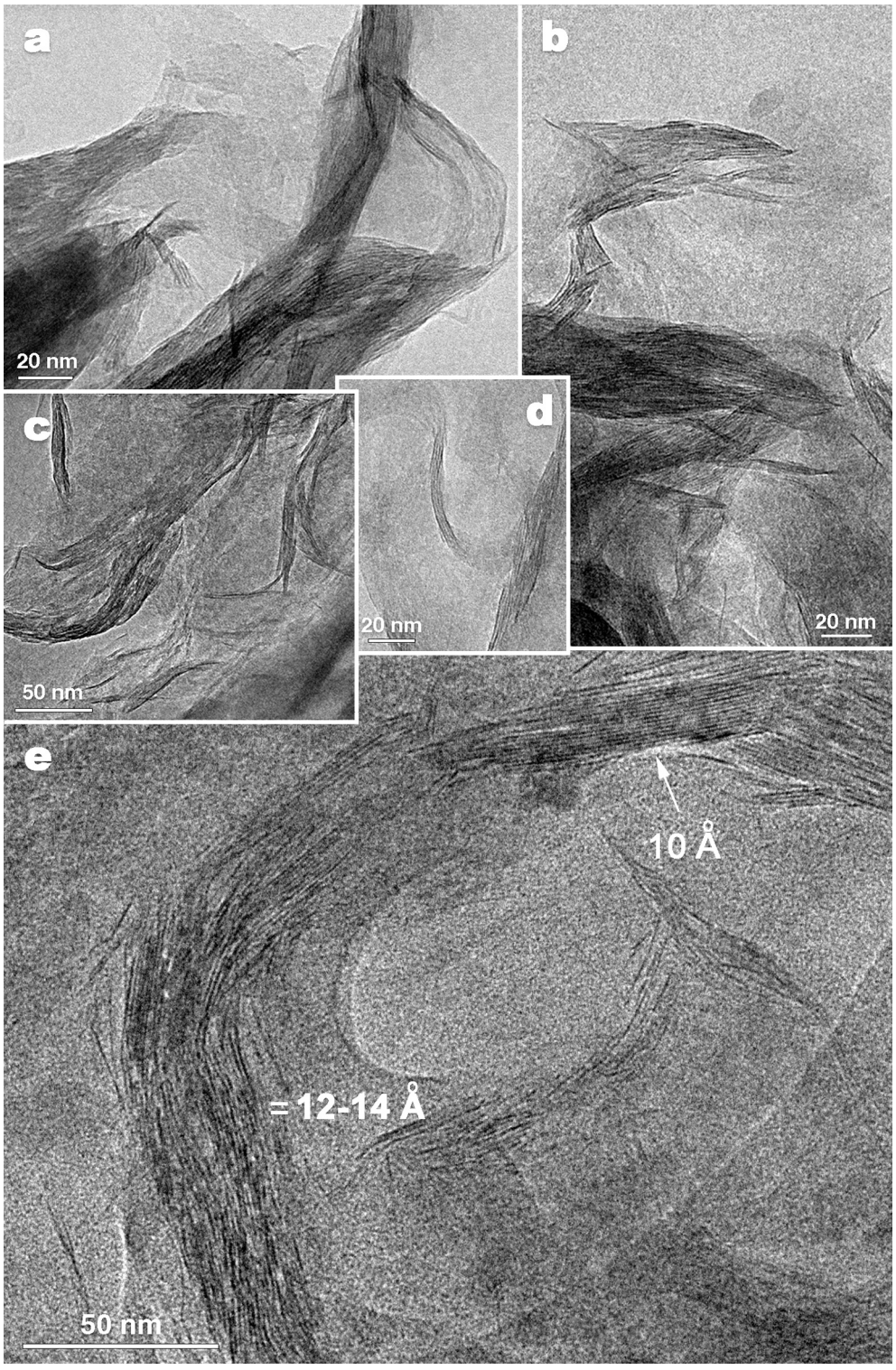

Fig. 5. TEM images of nanoparticles with variable morphology, continuously curved with a general wavy and pointy appearance and twister ends of Green Clays (a, b, e) and Pink Clays (c, d). Note the remarkable small size of particles in the Pink Clays samples (c, d). e) disordered smectitic mass (≈2–14 Å layers) containing residual illitic crystals (relatively defect-free 10-Å layers). (For interpretation of the references to colour in this figure legend, the reader is referred to the web version of this article.)

Green Clay samples. They were more resistant to the electron beam, so they were easily distinguishable because they were highlighted within the smectitic layers. They comprised straight parallel layer domains but usually showed marked signs of alteration. The illite particles generally appeared to be surrounded by extensive areas of a smectitic nature. In addition to edge dislocations, they frequently showed changes in image contrast along layers, including layers of more than 10 Å d-spacing within the 10 Å sequence (Fig. 7b), which was a consequence of a physical breakdown process that could be interpreted as exfoliation or microdivision perpendicular to the stacking direction. Other than the small illite or chlorite relics, the layers rarely had a continuity of more than a few nm (Figs. 6a, 7a), the d-spacing was variable, and the edge dislocations were observed along all the crystals (Fig. 7a). The general trend in the HRTEM images of the smectititc particles of both Pink Clays and Green Clays was disorder and small-sized particle.

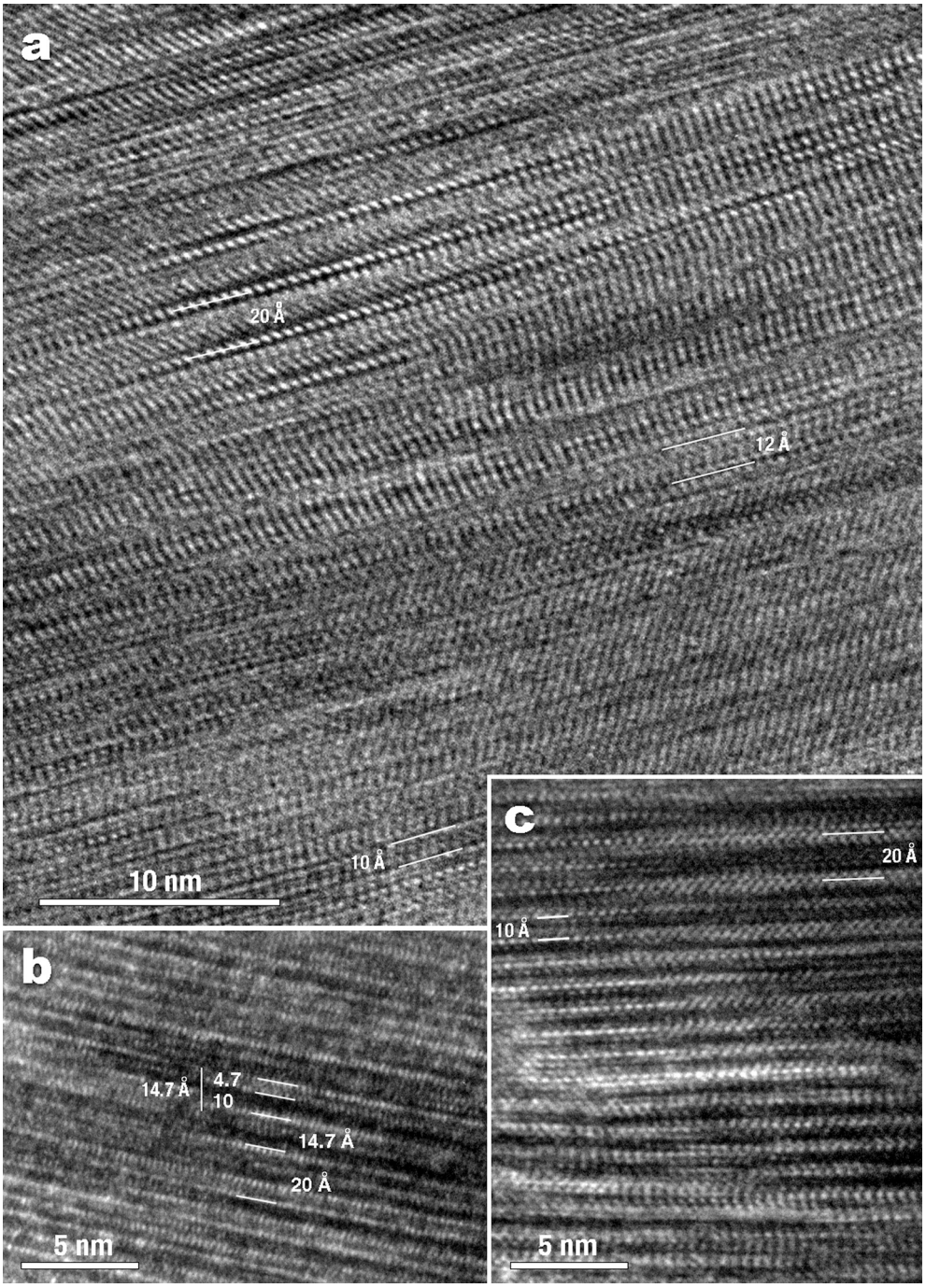

Fig. 6. HRTEM images. a) representative lattice-fringe images of the dominant disordered clay mass. The d-spacing varies from 10 to more than 20 Å, in disordered domains of only a few layers with lack of staking in [001] direction and scarce lateral continuity. b) straight parallel 14 Å layers (chlorite relict) with signs of alteration. c) d-spacing variation from 10 to more than 20 Å.

5. Discussion

The positive correlation between Al_2O_3, Fe_2O_3, and K_2O (Table 3 complementary material) was related to samples of higher oxide content. Point analyses of these compositions corresponded to those of groups A1 and A2 obtained in the cluster analysis (Table 2, Fig. 8d). The structural formulas of group A1 do not fit properly as dioctahedral mica because a high excess of octahedral charge (+0.39) was obtained. The excess octahedral charge after homoionization could be related to the presence of HIMs which are 2:1 phyllosilicates with oligomers in their interlayers. The hydroxy-interlayer is not a complete octahedral sheet, but it forms "islands" (Barnhisel and Bertsch, 1989) with a variable number of Al^{3+}, Mg^{2+}, or Fe^{3+} cations. The HIMs are secondary minerals from the alteration of the parent material, which are mainly present in soils (Meunier, 2005; Georgiadis et al., 2020). In the bentonites from the Tajo Basin, HIMs are the result of an intermediate stage in the alteration and transformation of micas and chlorites toward smectites. They are responsible for some of the discontinuous and irregular lattice fringes observed in the HRTEM images. Considering that part of MgO, Fe_2O_3, and Al_2O_3 proportion can be present in the interlayer oligomers of HIMs, part of the cations fitted as octahedral cations in the structural formula should be located in the interlayer space. Therefore, these particles must be more dioctahedral than that estimated from the structural formulas (4.72 Σ oct.). The intermediate stage in the alteration of micas is

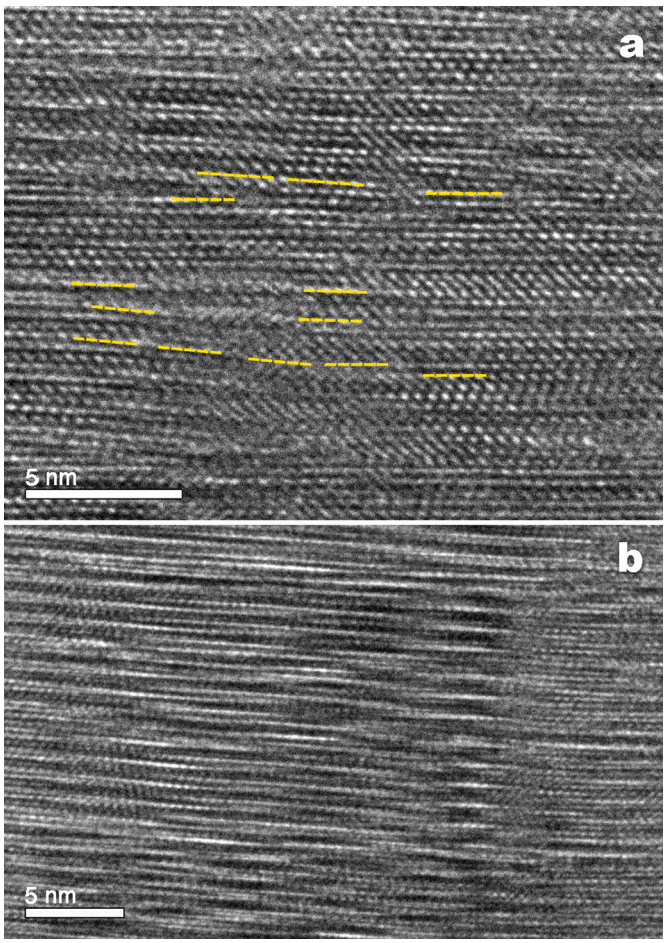

Fig. 7. HRTEM images of representative lattice-fringe showing changes in the image contrast along layers. The edge dislocations are disposed along all the crystals. b) residual illitic crystal showing changes in the image contrast along layers and include layers of more than 10 Å d-spacing within the 10 Å sequence.

supported by the K_2O content found in some analyses of group A1, which indicates interlayered illitic layers. Some point analyses with low SiO_2 values (less than 50%), high Fe_2O_3 (approximately 10–20%), should be related to the very low-intensity 14 Å reflections both in AO, AO + EG, and AO + TT DRX (Fig. 2 and Fig. 6b). Those reflections should be attributed to the remains of weathered chlorite from the source area, indicative of the intense alteration of chlorite, which is degraded almost. These chloritic particles are scarce in the Green Clays and hardly ever appear in the Pink Clays.

Cluster A2 was similar to A1. However, point analyses of this composition fit beidellite (Σ oct. 4.29) (Table 2), with some interlayered illitic layers, which is supported by the interlayer K^+ (0.31 p.u.c.). They represent intermediate phases and should be associated with the 10 Å and 1.49 Å reflections in the XRD patterns and with the scarce illitic relicts or illitic domains identified with HRTEM (Fig. 5e). Particles corresponding to groups A1 and A2 are the majority in the Green Clays.

The two A groups include primary phyllosilicate particles that are partially altered and transformed. The B group includes more evolved particles and is subdivided in three other subgroups. The B1 group of the cluster has a mean composition that is quite similar to group A particles but with minor K_2O, Al_2O_3, and Fe_2O_3 and higher MgO content. Its mean composition fit saponite although, the mean values are the results of a very wide compositional variation where both extremes are closer to saponite, muscovite, or mixed-layers of illite/smectite, which can be found even in the same sample (Fig. 6a). They are the result of the progression of mica alteration and the relative increase in Mg. Higher the mica alteration degree, lower K_2O, Al_2O_3, and Fe_2O_3 content and higher SiO_2 and MgO. This compositional variation is clearly reflected in the data plotted in Fig. 8d. These particles are mainly smectitic but contain illitic domains, as shown in the HRTEM images (Figs. 5, 6, and 7), and they are responsible for both the intense and broad reflections that appear around 14–15 Å in the AO (which expand to 17 Å following solvation with ethylene glycol and collapse to 10 Å upon heating to 550 °C, a typical behavior of smectites), and of the asymmetric 10 Å open to higher d-spacing XRD reflections, as well as some of the low-intensity effects of intermediate d-spacing between 10 and 14 Å. The number of octahedral cations, with a mean value of 5.39 p.u.c, as well as the 060 XRD reflections at both 1.49 Å and 1.52 Å, confirm the coexistence of trioctahedral (smectitic) and dioctahedral (illitic) domains.

Particles with a range of chemical compositions from near-mica and to those of mixed-layer illite/smectite or even smectite without a compositional gap (Fig. 2) between groups A1, A2, and B1 are more abundant in the Green than in the Pink Clays (Fig. 8).

Groups B211 and B212 have lower Al_2O_3, Fe_2O_3, and K_2O proportions and an increase in MgO, which is in good agreement with the negative correlation between MgO, Al_2O_3, and the other oxides; they are the richest in Mg, with a structural formula (from the mean of analyses) that fits as saponite with 6.04 and 5.58 Σoct. for B211 and B212, respectively (Table 2). The difference between the two groups is the small excess of octahedral charge and octahedral cations in the mean structural formula, and slightly more MgO and less Al_2O_3 in B212 than in B211, which is most likely related to small amounts of relict HIMs in B211. They represent a more advanced step in the process of the primary phyllosilicate alteration and transformation toward new magnesian phases. The Pink Clays mostly comprise slight stacking, disordered, and extremely poor crystallinity smectites with these compositions (B211 and B212). However, they hardly ever appear in Green Clays (Fig. 8b, d), and they produce very broad diffraction effects in the absence of a clear 001 reflection in the XRD patterns, which is related to the lack of three-dimensional periodicity. Further, they only contain small coherent diffraction domains in the [001] direction. This is evidenced by the HRTEM images because the nanoparticles often are composed of only a few stacked layers (Fig. 5c, d), resulting in very open microstructures.

The richest SiO_2 point analyses have also very high MgO percentages and scarce amounts of other chemical elements, and they are grouped into the B22 group. The mean structural formula does not fit as layer 2:1 phyllosilicate, it fits more properly as sepiolite (Table 2). This composition is closer to sepiolite, related to the fibrous ends that smectitic particles sometimes have (Fig. 4g, h). They are particles at the end of the transformation process, probably with epitactit growth of neoformed sepiolite on smectite crystals. They appear both in Green and Pink Clays but are much more prominent among Pink Clays the latter.

The continuous compositional variation (Figs. 3 and 8) indicates a mineralogical evolution, describing the genetic relationship between the mineralogical groups. It implies the evolution from primary phyllosilicates (micas and chlorites) to the final product, the very low-charge saponites and sepiolite. In the last stage, neoformation also occurs because the environment is enriched in Mg and Si. The Green Clays are richer in detrital minerals such as quartz and feldspars, and in intermediate phases such as HIMs and random illite/smectite mixed-layers while the Pink Clays are principally formed by very small particles enriched in Si and Mg, which correspond to very low-charge saponite together with scarce random smectite/illite mixed-layers close to the sepiolite-composition particles (Fig. 8a, b). Most point analysis of particles of the Green Clay samples are group in the A1, A2, and B1 clusters, while the analysis corresponding at samples of Pink Clays falls in the different subgroups of the B2 group defined by the statistical analysis (Fig. 8c, d).

The particles in which smectitic and illitic domains are identified by HRTEM are the most frequent, being more smectitic as they become more distal. The domains have sufficient size to diffract as a mixture of smectite and illite, such as individual particles but they are mixed-

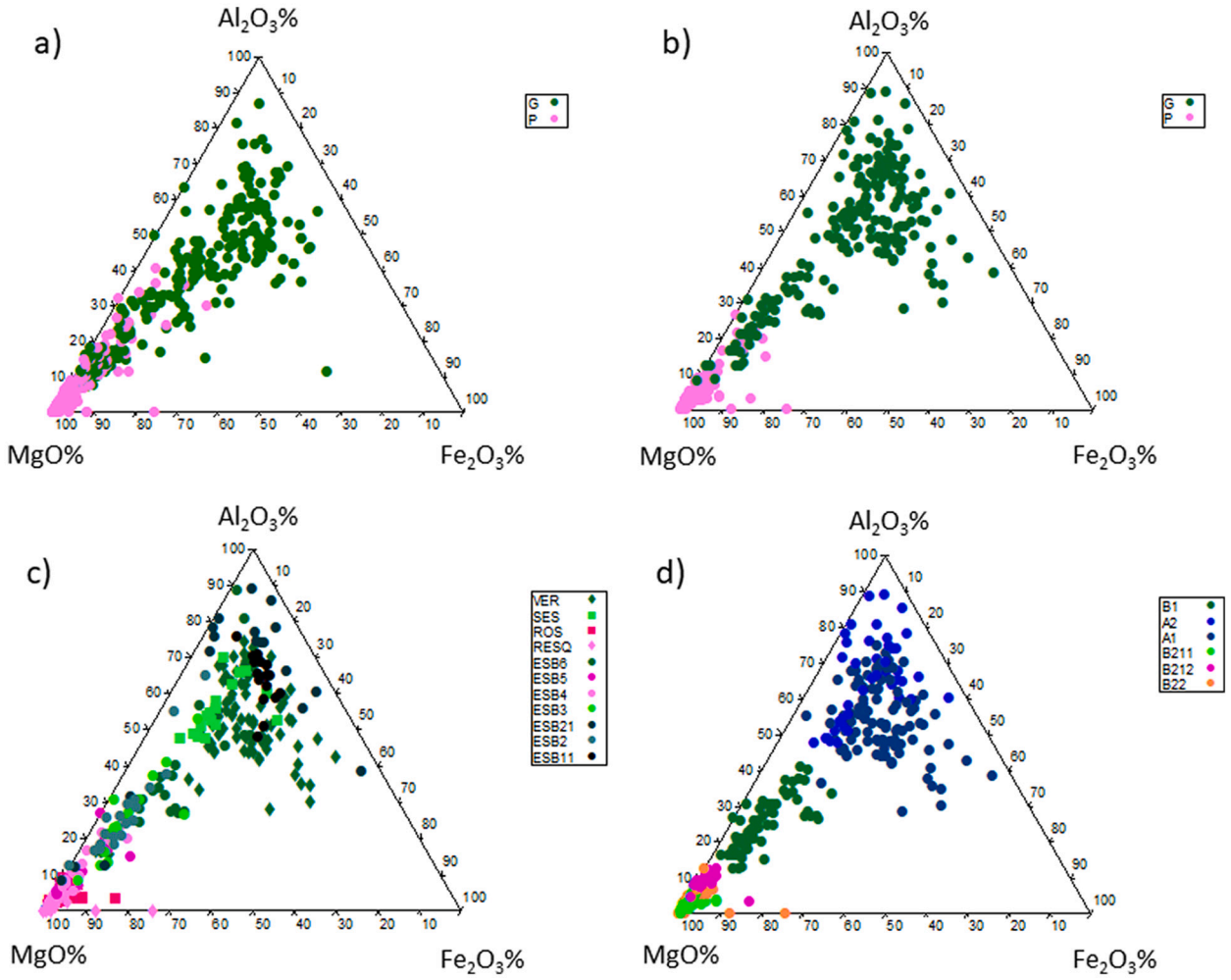

Fig. 8. Triangular plots of the relative proportions of the three main octahedral cations, expressed as percentage of oxides. a) natural samples, b) homoionized with Ca samples, G = Green Clays, P = Pink Clays, c) point analysis identified by samples (obtained in homoionized with Ca), and d) point analyses identified by groups (obtained in homoionized with Ca samples). (For interpretation of the references to colour in this figure legend, the reader is referred to the web version of this article.)

layers, which can change not only in the staking direction but laterally. Most previous works on the genesis of bentonites from the Tajo Basin propose from XRD pattern interpretation a mixture of illite as an inherited mineral and smectite as a neoformed mineral (Doval et al., 1985; Domínguez Díaz et al., 1997; García-Romero et al., 1990; De Santiago et al., 1998). However, the observations from this work for samples from different locations allow us to confirm that illitic particles are very scarce in Green Clays and they do not exist in Pink Clays although in the XRD patterns of both types of bentonites, a clear peak at 10 Å appears, which is more intense in the Green Clays. This diffraction effect is due to the illitic domains that appear in mixed particles, which are more smectitic farther from the source area of the deposit.

The formation of trioctahedral smectites from primary phyllosilicates has been determined previously for Green Clays. De Santiago et al. (1998) studied the weathering process of illite to form smectite and intermediate stages in the Green Clays of the Tajo Basin. They described how detrital illite transforms to smectite, which begins as an exfoliation normal to the stacking direction and develops by opening of the interlayer spacing, similar to Fig. 7b. These units evolve by disconnecting from the parent crystal as the cleavage process advances. They also described random mixed-layer illite/smectite as an intermediate product of this alteration process, as well as the replacement of K^+ by hydrated interlayer cations and slight reorganization of the 2:1 layer structure. Fesharaki et al. (2007) found a mixture of detrital (quartz, feldspars, kaolinite, micas, and chlorite) transformed (illite and beidellite) and neoformed (montmorillonite) minerals in the arkoses (more proximal facies) in the Miocene sediments of the Tajo Basin. These confirmed that the clay minerals resulted from interactions between detrital minerals and meteoric waters. The assemblage of dioctahedric minerals (illite and smectites) described by Fesharaki et al. (2007) evolved into a more trioctahedric composition in the distal facies of the basin. Conversely, the genesis of the Pink Clays has been related to neoformation by direct precipitation from rich in silica and magnesium solutions in the more distal facies in small ponds or playa lake environments (Doval et al., 1985; García-Romero et al., 1990; De Santiago et al., 1998, 2000; Pozo and Casas, 1999; Herranz and Pozo, 2018). Based on the very small crystal size, numerous edge dislocations, the lack of periodicity (turbostratic) in the structure, and a cellular (spherical) texture observed by HRTEM, the Pink Clays were considered to be an early stage of crystallization (De Santiago et al., 2000) in which trioctahedral smectites, described as a stevensite precursor, grow from colloidal phases enriched in the Mg and Si products of the weathering of mica and chlorite. However, the data here show evidence of a genetic relationship between Green and Pink Clays as different steps of a continuous alteration process.

The process of Green and Pink Clays formation began in the source area where the mica and chlorite alteration started. The alteration and transformation processes occurred through a series of irreversible

reactions during all stages of the sedimentary process and during the early diagenesis, where interstitial fluids could react with highly transformed detrital minerals; the growth of neoformed also happened, but in minor amounts. The transformations led to a progressive enrichment in Mg and Si of the new clay minerals in the more evolved materials. The enrichment in these elements already were reported by Domínguez Díaz et al. (1997) and De Santiago et al. (1998). During the entire transformation process of the mica and chlorite to smectite, there was an oxidation of Fe^{2+} to Fe^{3+} that forced the ejection of a third of the octahedral Fe^{3+} to avoid the excess of octahedral charge after Fe oxidation. The chemical and structural rearrangement resulted from the release of Fe^{3+}, provoking the relative Mg and Si enrichment in the newly formed minerals (Gilkes et al., 1972), which was corroborated by the positive correlation between SiO_2 and MgO. This must contribute to the high proportions of Si and Mg occurring in the more evolved Tajo Basin sediments, because those richest in Al and Fe phyllosilicates remained in the more proximal facies, as described by Fesharaki et al. (2007). The Green Clays have large Fe_2O_3 variability (Table 1, Fig. 8a, b), which was absent in some smectite particles; however, it can reach 21.88% in some other particles, in those that are the less evolved phyllosilicates in the sequence of alteration–neoformation from the micas to the low-charge saponite and sepiolite. This variability can be related to some of the octahedral Fe^{3+} and tetrahedral Al^{3+} being ejected from mica and chlorite remaining as hydroxy-interlayers in the alteration products. The process occurs in both Green and Pink Clays, but it is a majority in the former and less important the latter, representing a more evolved sediment.

The HRTEM images indicate that the transformation from parent minerals to clay minerals in the Green Clays is mainly an atom-to-atom transformation in the solid state. Although, local dissolution and crystallization could also occur. There is no evidence of the local dissolution and crystallization process, but, on the contrary, the degradation of mica (Fig. 7b) and chlorite (Fig. 6 b) is observed by the opening of the interlayer spacing with slight a reorganization of the 2:1 layer structure. Consequently, there are remains of illite particles (straight and relatively defect-free lines) surrounded by extensive areas of smectite (imperfect and wavy fringes) and hydroxy-interlayer minerals and random mixed-layers as uncompleted stages in the transformation (Fig. 5e). They have a high density of edge dislocations, which may serve as diffusion pathways.

Green Clays correspond to the state of transformation to smectites where detrital components are still predominant, with intermediate phases between primary minerals (micas and chlorites) and final products (very low-charge saponite and sepiolite), while Pink Clays represent most evolved stages in the mineral transformation in which neoformation can also occur in an ambience enriched in Si and Mg. The alternation of Green and Pink Clay levels should be related to climatic changes with alternations of humid and arid periods that produce variation in the contribution of the detrital components to the lake, with the progradation or retrogradation of the more proximal facies over the more distal ones. The wettest periods lead to the higher hydrolysis and mobilization of minerals from the source area to the basin creating the Green Clays while Pink Clays represent more distal facies, and they could be related to more arid periods with minor detrital contributions of smaller and very altered particles, with high concentrations in Si and Mg that could lead to Mg-smectites by transformation and neoformation of sepiolite in the last term.

6. Final remarks and conclusions

The sedimentary deposits of bentonites of the Tajo Basin resulted in a complex clay mineral assemblage due to the sum of processes during the weathering of parent rocks and the evolution of the materials in in the sedimentary environment. Green and Pink Clays are bentonites comprising a mix of laminar nanoparticles of mainly 2:1 phyllosilicates, with a mean structural formula close to a low-charge trioctahedral smectite that appears together with some scarce other detrital inherited minerals such as quartz, feldspars, and kaolinite, although wide variations in the crystal chemistry of the clay particles is the main characteristic in all studied samples.

The wide compositional and microstructural variations are the main characteristic of these clay minerals. Nonetheless, they have been statistically classified in groups that represent the evolution from the primary phyllosilicates (dioctahedral and trioctahedral micas, and chlorites) to very low-charge trioctahedral saponite and sepiolite. The intermediate steps in this transformation involve particles with structural formulas that have an excess of octahedral cations and that are interpreted as HIMs and random interlayers of illite/smectite, which are poorer in illitic components the more evolved the particle is. Green Clays are much richer in HIMs and illitic layers interstratified in smectites, which is conducive to higher charge 2:1 particles compared to Pink Clays. The Pink Clays are richer in more evolved smectitic particles with a composition of low-charge saponite that is close to stevensite or kerolite, as well as small amounts of particles with the composition of sepiolite.

The progressive compositional variation from the inherited or precursor minerals (mainly micas but also chlorite) to the neoformed (saponite–stevensite and sepiolite) represents a noticeable relative increase in SiO_2 and MgO content together a decrease of the other oxides. Pink Clays correspond to more distal facies in which the transformation of primary minerals is higher. While microstructural changes occur in phyllosilicates, the crystal chemistry of the particles also change; the more proximal facies (Green Clays) are relatively enriched in Al, Fe and K, while the more distal ones (Pink Clays) are enriched in Mg and Si. The presence of beds of Pink Clays stratified among the more abundant Green Clays in the Green Clays Unit could represent periods of more arid conditions, with a minor contribution of relatively lesser evolved detrital material to the basin.

Author contributions

Both authors have contributed equally and agreed to the entire version of the manuscript.

Declaration of Competing Interest

The authors declare that they have no known competing financial interests or personal relationships that could have appeared to influence the work reported in this paper.

Acknowledgements

Grant PID-2019-106504RB funded by MCIN/AEI/ 10.130 39/ 501100011033.

Appendix A. Supplementary data

Supplementary data to this article can be found online at https://doi.org/10.1016/j.clay.2022.106515.

References

Alonso-Zarza, A.M., Calvo, J.P., Silva, P.G., Torres, T., 2004. Cuenca del Tajo. In: Vera, J. A. (Ed.), Geología de España. SGE-IGME, pp. 556–561.
Aspandiar, M.F., Eggleton, R.A., 2002. Weathering of chlorite: I. Reactions and products in microsystems controlled by the primary mineral. Clay Clay Miner. 50 (6), 685–698.
Banfield, J.F., Eggleton, R.A., 1988. Transmission electron microscope study of biotite weathering. Clay Clay Miner. 36 (1), 47–60.
Banfield, J.F., Eggleton, R.A., 1990. Analytical transmission electron microscope studies of plagioclase, muscovite, and K-feldspar weathering. Clay Clay Miner. 38 (1), 77–89.
Barnhisel, R.I., 1977. Chlorites and Hydroxy Interlayered Vermiculite and Smectite. In: Dixon, J.B., Weed, S.B., Kittrick, J.A., Milford, M.H., White, J.L. (Eds.), Minerals in Soil Environments. SSSA, Madison, WI, USA, pp. 331–356.

Barnhisel, R.I., Bertsch, P.M., 1989. Chlorites and hydroxyinterlayered vermiculite and smectite. In: Dixon, J.B., Weed, S.B. (Eds.), Minerals in Soil Environments. Soil Science Society of America, Madison (WI, USA), pp. 728–788.
Bellanca, A., Calvo, J.P., Censi, P., Neri, R., Pozo, M., 1992. Recognition of lake-level changes in Miocene lacustrine units, Madrid Basin, Spain. Evidence from facies analysis, isotope geochemistry and clay mineralogy. Sediment. Geol. 76, 135–153.
Brell, J.M., Doval, M., Carames, M., 1985. Clay minerals distribution in the evaporitic Miocene sediments of the Tajo Basin, Spain. Mineral. Petrogr. Acta 29, 267–276.
Buurman, P., Meijer, E.L., van Wijck, J.H., 1988. Weathering of chlorite and vermiculite in ultramafic rocks of Cabo Ortegal, northwestern Spain. Clay Clay Miner. 36, 63–269.
Calvo, J.P., Ordoñez, S., García del Cura, M.A., Hoyos, M., Alonso-Zarza, A.M., Sanz, E., Rodríguez Aranda, J.P., 1989a. Sedimentología de los complejos lacustres miocenos de la Cuenca de Madrid. Acta Geol. Hisp. 22 (3–4), 281–298.
Calvo, J.P., Alonso-Zarza, A.M., García del Cura, M.A., 1989b. Models of marginal lacustrine sedimentation in response to varied source areas in the Madrid Basin (Central Spain). Paleogeogr. Paleoclimatol. Paleoecol. (70), 199–214, 1989.
Calvo, J.P., Daams, R., Morales, J., López-Martínez, N., Agustí, J., Anadón, P., 1993. Up-to-date Spanish continental Neogene synthesis and paleoclimatic interpretation. Rev. Soc. Geol. Esp. 6, 29–40.
Clauer, N., Fallick, A.E., Galán, E., Pozo, M., Taylor, C., 2012. Geochim. Cosmochim. Acta 94, 181–198.
Correns, C.W., 1963. Experiments on the decomposition of silicates and discussion of chemical weathering. Proc. 10th Natl. Conf. Clays Clay Miner. 443–459.
Craw, D., 1984. Ferrous-iron-bearing vermiculitesmectite series formed during alteration of chlorite to kaolinite, Otago schist, New Zeland. Clay Miner. 19, 509–520.
Cuevas, J., Pelayo, M., Rivas, P., Leguey, S., 1993. Characterization of Mg-clays from the Neogene of the Madrid Basin and their potential as backfilling and sealing material in high level radioactive waste disposal. Appl. Clay Sci. 1993 (7), 383–406.
Cuevas, J., De La Villa, R.V., Ramirez, S., Petit, S., Meunier, A., Leguey, S., 2003. Clay Clay Miner. 51, 457–472.
Cuevas, J., Fernández Barrenechea, J., García-Romero, E., Leguey, S., Luque, J., 2010. Field trip guide and abstracts of the sepiolite symposium. 2010 SEA-CSSJ-CMS Trilateral Meeting on Clays. June 7th, 2010, Madrid-Seville, Spain. Cuevas, J.; Barrenechea, J.F.; García-Romero, E.; Leguey, S- Luque, J. (Eds.), 65 pp.
De Santiago, C., Suárez, M., García-Romero, E., Domínguez Díaz, M.C., Doval, M., 1998. Electron microscopic study of the illite–smectite transformation in the bentonites from Cerro Del Aguila (Toledo, Spain). Clay Miner. 33, 501–510.
De Santiago, C., Suárez, M., García-Romero, E., Doval, 2000. Mg-rich smectite "precursor" phase in the Tagus Basin, Spain. Clay Clay Miner. 48 (3), 366–373.
Dixon, J.B., Jackson, M.L., 1962. Properties of intergradient chlorite-expansible layer silicates of soils. Soil Sci. Soc. Am. J. 26, 358–362.
Domínguez Díaz, M.C., Brell, J.M., Doval, M., García-Romero, E., 1997. Análisis de los minerales de la arcilla y sus procesos genéticos en las formaciones arcillosas de la cuenca del Tajo. Estud. Geol. 53, 185–196.
Doval, M., Domínguez Díaz, M.C., Brell, J.M., García-Romero, E., 1985. Mineralogía y sedimentología de las facies distales del borde norte de la Cuenca del Tajo. Bol. Soc. Esp. Mineral. 257–269.
Elsass, F., Srodon, J., Robert, M., 1997. Illite-smectite alteration and accompanying reactions in a Pennsylvanian underclay studied by TEM. Clay Clay Miner. 45 (3), 390–403.
Fesharaki, O., García-Romero, E., Cuevas-González, J., López-Martinez, N., 2007. Clay mineral genesis and chemical evolution in the Miocene sediments of Somosaguas, Madrid Basin, Spain. Clay Miner. 42, 187–201.
García-Rivas, J., Suárez, M., Torres, T., Sánchez-Palencia, Y., García-Romero, E., Ortiz, J. E., 2018. Geochemistry and biomarker analysis of the bentonites from Esquivias (Toledo, Spain). Minerals 8, 291.
García-Romero, E., Suárez, M., 2018. A structure-based argument for non-classical crystal growth in natural clay minerals. Min. Mag. 82 (1), 171–180.
García-Romero, E., Suárez, M., 2021. The alteration of Miraflores Basalt (Panama): Mineralogical and textural evolution. Appl. Clay Sci. 205, 106036.
García-Romero, E., Brell, J.M., Doval, M., Navarro, J.V., 1990. Caracterización mineralógica y estratigráfica de las formaciones neógenas del borde sur de la cuenca del Tajo (Comarca de la Sagra). Bol. Geol. Min. 101–106, 945–956.
García-Romero, E., Manchado, E.M., Suárez, M., García Rivas, J., 2019. Spanish bentonites: a review and new data on their geology, mineralogy, and crystal chemistry. Minerals. 9, 696.
García-Romero, E., Lorenzo, A., García-Vicente, A., Morales, J., García-Rivas, J., Suárez, M., 2021. On the structural formula of smectites: a review and new data on the influence of exchangeable cations. J. Appl. Crystallogr. 54, 251–262.
Georgiadis, A., Dietel, J., Dohrmann, R., Rennert, T., 2020. Review Article. What are the nature and formation conditions of hydroxy-interlayered minerals (HIMs) in soil? J. Plant Nutr. Soil Sci. 183, 12–26.
Gilkes, R.J., Young, R.C., Quirk, J.P., 1972. The oxidation of octahedral iron in biotite. Clay Clay Miner. 20, 303–315.
Gupta, G.C., Malik, W.U., 1969. Fixation of hydroxy-aluminium by montmorillonite. Am. Mineral. 54, 1625–1634.
Güven, N., Kerr, P.F., 1966. Weathering effects of the structures of mica-type clay minerals. Am. Mineral. 51, 858–874.
Herranz, J.E., Pozo, M., 2018. Authigenic Mg-clay minerals formation in lake margin deposits (the Cerro de los Batallones, Madrid Basin, Spain). Minerals 8, 418.
Hervillon, A.J., Makumbi, M.N., 1975. Weathering of chlorite in a soil derived from a chloritoschist under humid tropical conditions. Geoderma 13 (2), 89–104.
Hoang-Minh, T., Kasbohm, J., Nguyen-Thanh, L., Nga, P.T., Lai, L.T., Duong, N.T., Thanh, N.D., Thuyet, N.T.M., Anh, D.D., Pusch, R., Knutsson, S., Ferreiro Mählmann, R., 2019. J. Appl. Crystallogr. 52, 133–147.
Junco, F., Calvo, J.P., 1983. Cuenca de Madrid. In: Libro Jubilar, J., Ríos, M. (Eds.), Geología de España, II, pp. 534–542.
Klimentidis, R.E., 1986. High resolution imaging of ordered mixed-layer clays. Clay Clay Miner. 34, 155–164.
Kogure, T., Murakami, T., 1996. Direct identification of biotite/vermiculite layers in hydrobiotite using high-resolution TEM. Min. J. 18 (4), 131–137.
Malström, M., Banwart, S., 1997. Biotite dissolution at 25°C: the pH dependence of dissolution rate and stoichiometry. Geochim. Cosmochim. Acta 61 (14), 2779–2799.
Martín de Vidales, J.L., Pozo, M., Alia, J.M., García Navarro, F., Rull, R., 1991. Kerolite-stevensite mixed-layers from the Madrid Basin, Central Spain. Clay Miner. 26, 329–342.
Meunier, A., 2005. Clays. Springer, 476 pp.
Mukarami, T., Isobe, H., Sato, T., Ohnukim, T., 1996. Weathering of chlorite in a quartz-chlorite schist: I. Mineralogical and chemical changes. Clay Clay Miner. 44, 2, 244–256.
Ordoñez, S., Calvo, J.P., García del Cura, M.A., Alonso Zarza, A.M., Hoyos, M., 1991. Sedimentology of sodium sulphate deposits and special clays from the Tertiary Madrid Basin (Spain). In: Anadón, P., Cabrera, L., Kelts, K. (Eds.), Lacustrine Facies Analysis, pp. 39–55. Spec. Publ. Int. Assoc. Sedimentol.13.
Pozo, M., Calvo, J.P., 2015. Madrid Basin (Spain): A natural lab for the formation and evolution of magnesian clay minerals. 229–282. In: Pozo, M., Galán, E. (Eds.), Magnesian Clays. Characterization, Origin and Applications. AIPEA Educational Series, Puib. N° 2. Digilabs. Bari, Italy, 380 pp.
Pozo, M., Casas, J., 1992. Mineralogía y sedimentología del yacimiento de saponita de Yuncos (Toledo). Estud. Geol. 48, 47–65.
Pozo, M., Casas, J., 1995. Distribución y caracterización de litofacies en el yacimiento de arcillas magnésicas de Esquivias (Neógeno de la Cuenca de Madrid). Bol. Geol. Min. 106, 265–282.
Pozo, M., Casas, J., 1999. Origin of kerolite and associated Mg clays in palustrine-lacustrine environments. The Esquivias deposit (Neogene Madrid Basin, Spain). Clay Miner. 34, 395–418.
Pozo, M., Galán, E., 2015. Magnesian Clay deposits: mineralogy and origin. 175–228. In: Pozo, M., Galán, E. (Eds.), Magnesian Clays. Characterization, Origin and Applications. AIPEA Educational Series, Pub. N° 2. Digilabs. Bari, Italy, 380 pp.
Pozo, M., Casas, J., Martín De Vidales, J.L., Medina, J.A., Martín Rubí, J.A., 1999. Características texturales y composicionales en depósitos de arcillas magnésicas de la (Cuenca de Madrid. I) Kerolitas (sector de Esquivias y Pinto). Bol. Geol. Min. 110–111, 77–102.
Proust, D., 1982. Supergene alteration of metamorphic chlorite in an amphibolite from Massif Central, France. Clay Miner. 17, 159–173.
Proust, D., Dudoignon, P., Bouchet, A., Meunier, A., 1987. Marine and supergene alteration progresses in a chloritized amphibole-schist, Deux-Serves, France. Clay Miner. 22, 129–143.
Rimmer, S.M., Eberl, D.D., 1982. Origin of an underclay as revealed by vertical variations in mineralogy and chemistry. Clay Clay Miner. 30 (6), 422~130.
Robert, M., 1973. The experimental transformation of mica toward smectite; relative importance of total charge and tetrahedral substitution. Clay Clay Miner. 21, 167–174.
Robert, M., Barshad, I., 1973. Variability of interlayered d(001) spacing of experimentally opened micas: its significance on the identification and classification of 2/1 expanding clay minerals. Clay Clay Miner. 21, 1463–1465.
Romero, R., Robert, M., Elsass, F., García, C., 1992. Evidence by transmission microscopy of weathering microsystems in soils developed from crystalline rocks. Clay Miner. 27, 21–33.
Ross, G.J., Wang, C., Ozkan, A.I., Rees, H.W., 1982. Weathering of chlorite and mica in a new Brunswick Podzol developed on till derived from chlorite-mica schist. Geoderma 27 (3), 255–267.
Srodón, J., Eberl, D.D., 1984. Illite. In: Bailey, S.W. (Ed.), Micas. Rev Mineral 13. Mineral Soc. Am, Washington, DC, pp. 495–544.
Steudel, A., Friedrich, F., Schuhmann, R., Ruf, F., Sohling, U., Emmerich, K., 2017. Characterization of a fine-grained interstratification of turbostratic talc and saponite. Minerals 7 (1), 5.
Suarez, M., Robert, M., Elsass, E., Pozas, J.M., 1994. Evidence of a precursor in the neoformation of palygorskite–New data by analytical electron microscopy. Clay Miner. 29, 255–264.
Tessier, D., 1984. Etude de l'organisation des matériaux argileux. Hydration, gonflement et structuration au cours de la dessiccation et de la rehumectation. Thèse de Docteurès Sciences de l'Unive. Paris VII, France.
Tessier, D., Pedro, G., 1987. Mineralogical characterization of 2:1 clays in soils: Importance of the clay texture. In: Shultz, S.G., van Olphen, H., s (Eds.), Proceedings of the International Clay Conference, Denver. The Clay Minerals Society, Bloomington, USA, pp. 78–84.
Veblen, D.R., Guthrie, G.D., Kenneth, J.R., Livi, J.T. (Eds.), 1990. Clay Clay Miner. 38, 1–13.
Velde, B., Meunier, A., 2008. The Origin of Clay Minerals in Soils and Weathered Rocks. Springer, 406 pp.
Wilson, W.J., 2004. Weathering of the primary rock-forming minerals: processes, products and rates. Clay Miner. 39, 233–266.